Article

Histomorphometric, Immunohistochemical, Ultrastructural and Statistic Biomaterial Evaluation: Comparison Between Synthetic Nano-hydroxyapatite /Beta-tricalcium Phosphate and Hydroxyapatite in No Critic Defects in Rat Calvaria

Igor da Silva Brum [1], Lucio Frigo [2], Renan Lana Devita [3], Jorge Luís da Silva Pires [4], Victor Hugo Vieira de Oliveira [5], Ana Lucia Rosa Nascimento [6] and Jorge José de Carvalho [7]

1. State University of Rio de Janeiro, Rio de Janeiro, RJ - Brazil, Carvalho@uerj.br
2. Universidade Guarulhos, Guarulhos, São Paulo – Brasil, luciofrigo@uol.com.br
3. State University Barcelona—Barcelona, Spain; doctornan28@gmail.com

[3] State University of Rio de Janeiro, Rio de Janeiro, RJ - Brazil, jorgepires45@gmail.com
[4] State University of Rio de Janeiro, Rio de Janeiro, RJ - Brazil, victorrhvoabio@gmail.com
[5] State University of Rio de Janeiro, Rio de Janeiro, RJ - Brazil, ana.nascimento@uerj.br
[6] State University of Rio de Janeiro, Rio de Janeiro, RJ - Brazil, jjcarv@gmail.com

* Correspondence: Igor_brum1@hotmail.com; Tel.: +55-(21)-988244976

Abstract: Nowadays, we can observe a worldwide trend towards the development of synthetic biomaterials. Several studies have been conducted to have a better understanding of the cellular conduct involved in the processes of inflammation and bone healing related to living tissues. The aim of this study is to evaluate tissue behavior of two different types of biomaterials: synthetic nano-hydroxyapatite / beta-tricalcium phosphate and hydroxyapatite in non-critical bone defects in rat calvaria. Twenty-four rats underwent experimental surgery procedure in which two 3 mm defects in each cavity were performed. Rats were divided into 2 groups: Group 1, using xenogen hydroxyapatite (Bio oss ™); Group 2, using synthetic nano-hydroxyapatite / beta-tricalcium phosphate (Blue Bone ™). Sixty days after surgery, calvaria bone defect was filled with biomaterial, animals were euthanized and stained with Masson's trichrome and PAS staining technic, immune-labeled with anti-TNF-α, anti-MMP-9 and electron microscopy analyzes were also performed. Histomorphometric analysis indicates a greater presence of protein matrix in Group 2, in addition to higher levels of TNF-α, MMP-9. The ultrastructural analysis shows biomaterial-fibroblasts association in tissue regeneration stage. Paired statistical data indicates that Blue Bone ™ can improve bone formation / remodeling when compared to biomaterials of xenogenous origin.

Keywords: Synthetic; xenogenous; nano-hydroxyapatite; beta-tricalcium phosphate

1. Introduction

Biomaterials evolution has provided countless discoveries in the area of guided bone-guided regeneration research field, allowing the development of bioactive materials, that means, nowadays it is possible to direct matrix deposition and reabsorption modulating cells involved in various tissue regeneration processes [1]. Among these materials, hydroxyapatites have been extensively studied, providing an extensive literature with new scientific evidence [2].

Currently, there are numerous hydroxyapatites (HA) from different sources available on the market and only a few biomaterials composed exclusively of beta-tricalcium phosphate (β-TCP). Bio oss ™, the world's leading hydroxyapatite product, from bovine origin (xenogen), presents 100% hydroxyapatite in its composition with a wide literature supporting its osteoconductor capabilities [3,4,5,6].

However, once biotechnology evolves, other materials have emerged, with different compositions and origins, aiming to provide genetic materials-free products, the so-called synthetics (alloplastics). Song et al, concluded that a combination of synthetic HA and ß - TCP in different proportions (ratios) could combine the rapid replacement by newly formed bone provided by β-TCP), with the slow absorption of hydroxyapatite, to maintain the volume of the grafted area [7].

In addition, nano-biotechnology has been studying not only the chemical relationship between nano-HA and nano-β-TCP, but also the fact that the nanometric structure could help in the ossification process. The powders have specific physicochemical and biological properties which, because of their nanometric dimension, large surface area, great interfacial compatibility and capacity to interact with the cells, promote: adhesion, migration, proliferation and cellular distinction [8,9]. Consequently, due to all these characteristics, other biomaterials have been developed, mixing nano-HA and nano (β-TCP) in different ratios, aiming to provide advantages of nano-technology-processed biomaterials over conventional HA, whether synthetic or xenogenic in relation to the processes of osteoconduction and osteoinduction [10].

There are basically two ways to analyze bone morphology: 1) isotopic collagen analysis (slightly less destructive and occasionally less accurate); and 2) histological analysis (less costly and destructive) [11]. Therefore, histological analyzes are indicated to determine and quantify innumerable biological characteristics, among them the formation of bone matrix, osteoblasts, osteocytes, osteoclasts, and pro-inflammatory factors, among others.

Through immunohistochemistry [12] it is possible to detect and quantify antigen-antibody signals and inflammatory mediators involved in the bone repair process. As an example, it can use markers such as MMP-9, TNF-α and PAS staining that are directly related to this process.

There are currently described 24 subtypes of metalloproteinases (MMPs) that are found in humans, rodents and amphibians [13]. MMP transcripts are commonly expressed at low-levels, but these levels can increase rapidly when tissues undergo remodeling, such as inflammation, wound healing and cancer. Particularly, MMP-9 (also known as gelatinase B), is a multi-domain enzyme that works in acute and chronic diseases related to inflammatory and neoplastic responses. The main cells responsible for secreting MMP-9 are macrophages and neutrophils [14]. One of the main reasons for studying MMP-9 is because it is essential to start the process of osteoclastic resorption where it triggers the process of removing the collagen layer from the bone surface before demineralization can begin [15].

Pro-inflammatory cytokines, such as interleukin IL-2, IL-6 and tumor necrosis factor α (TNF-α) are directly related to the process of bone resorption through inflammatory processes. In particular, the expression of TNF-α in areas of bone defects can disturb and impair bone regeneration [16]. TNF-α is produced by macrophages and many other cells, including CD4 + lymphocytes, neutrophils and mast cells [17].

PAS (Periodic Acid Schiff) technique is an important histological marker in the bone remodeling process, because it is used to mark bone growth [18]. Osteoblast organelles, which contain bone matrix precursors, are stained pink by the PAS technique [19]. PAS staining is an important method for labeling proteoglycans and collagen in the formation of the extracellular matrix. Recently researches have demonstrated the presence of several types of collagen and proteoglycans that are distinctly expressed in cartilage, in the passage from cartilage to bone and in extracellular bone matrixes. These discoveries indicate the complexity of the extracellular skeletal matrix, as well as its fluid expression. While the composition of cartilage and extracellular bone matrices is well-known, the function of each of the macromolecules that constitute these matrixes and their development regulation is not clearly comprehended [20,21].

Scanning Electron Microscopy (SEM) is used in the study of guided bone regeneration to identify and quantify cells or particles involved in the process. When it comes to hydroxyapatite, it is possible to use the SEM to measure its size, identifying its composition and distribution, through microanalysis [22].

The aim of the present study was to compare two biomaterials: nanohydroxyapatite / beta-tricalcium phosphate and hydroxyapatite in non-critical defects in rat calvaria in terms of

histomorphometric analysis using: Masson's trichrome and Periodic Acid Schiff staining, in addition to TNF- α and MMP-9-immunostaining and scanning electron microscopy.

2. Material & Methods

2.1. Animals

The experimental animal procedures protocol was approved by local Animal Ethics Committee (#001/2019). Forty-eight adults male *Wistar* rats, 200-220g of body weight, provided by Roberto Alcantara of the Biology Institute of Rio de Janeiro State University, were used. Animals were maintained in individual cages with *ad libitum* access to food and water. Light/dark cycle (lights on at 7:00 am, off at 7:00 pm) and temperature (22 °C) were kept constant. Rats were divided into two experimental groups (n = 24), after surgical procedures.

2.1.1. Bone defect surgical procedures

Rats were anesthetized with ketamine hydrochloride/xylazine solution (1/1, 0,1 mg/kg, i.p.). Dorsal cranium was trichotomized and a sagittal incision was carried out, using a sterile surgical scalp. Skin and periosteum were cleared in both parietal regions to proceed bone defects. Bone defects were achieved using a sterilized punch (cutting edge Ø 3 mm). Bone fragments were carefully removed to avoid damage of dura mater and related blood vessels. After biomaterial insertion in bone defects, the animal skin was carefully placed and sutured with cotton-wire.

2.1.2. Groups distribution

Rats were distributed into 2 groups: Group 1 (n = 24): bone defects were filled with 0,1g of hydroxyapatite (100%) (Bio Oss™, Geistlich, Switzerland); Grupe 2 (n = 24): bone defects were filled with 0,1g of nano-hydroxyapatite/beta-tricalcium phosphate complex (80/20%) (Blue Bone™, Regener, Brazil).

2.1.3. Euthanize procedure

Sixty days after biomaterials insertion, animals were euthanized under deep anesthesia: ketamine hydrochloride/xylazine solution (1/1, 0,3 mg/kg, i.p.). Animals were decapitated and the heads were followed with histological procedures.

2.2. Morphological analysis protocol

Animal heads were trimmed and decalcified in EDTA (7.0%) in PBS (0.1M, pH 7.4) for 40 days. Specimens were washed in distilled water, dehydrated in alcohol (70, 95, 100%), clarified in dimethylbenzene and embedded in paraffin (Paraplast™) at 65 °C. Serial sections of 7µm were cut, using a microtome (LEICA, Nussloch, Germany) and collected on silanized slides.

2.3. Masson's trichrome staining protocol

The slides were dewaxed and then rehydrated with alcohol (100, 95, 70%), rinsed in distilled water and immersed in Weigert's iron hematoxylin (Sigma-Aldrish) for 10 minutes. After being rinsed in distilled water, the slides were immersed in Biebrich fuchsin solution (Sigma-Aldrish) for 15 minutes, rinsed again in distilled water and differentiated in phosphomolybdovanic acid solution for 10 minutes. It was then submerged in aniline blue solution for 5 minutes, and a final rinse with distilled water, dehydration and coverslipping.

2.4. Immunohistochemistry protocol

Slides were deparaffinized, rehydrated and immersed in hydrogen peroxide (3%) to neutralize endogenous peroxidase, for 15 minutes. Sections were then washed in phosphate-buffered saline (PBS) and submitted to antigen retrieval using a citrate buffer solution, pH 6, heated at 60°C for 20 minutes. Unspecific antigen cross-reaction was ascertained using PBS-containing (3%) albumin bovine serum for 20 minutes. After, they were incubated with antibody anti-MMP-9 (1:200) (Santa Cruz Biotechnology Inc. USA), TNF-α (1:200) (Santa Cruz Biotechnology Inc. USA) in a humidified chamber at 4°C overnight. Sections were incubated using detection system VECTASTAIN® Universal Quick HRP Kit, revealed with DAB (3,3-diaminobenzidine) (Sigma-Aldrish) and counterstained with hematoxylin (Sigma-Aldrish).

2.5. Periodic Acid Schiff (PAS) protocol

Slides were deparaffinized and rehydrated through alcohol (100, 95, 70%), washed in distilled water and immersed in periodic acid (1%) for 5 minutes and rinsed in distilled water. Slides were immersed in Schiff's reagent [Fuchsin Basic (1%), Sodium metabisulphite (2%) in HCl (2%) solution] for 5-15 minutes, followed by a wash in running tap water for 5-10 minutes, and counter stained with Herri's hematoxylin for 15 seconds.

2.6. Image acquisition and histomorphometry

Three randomized slide fields in Masson's trichrome, PAS-stained and immune-labeled (TNF-α, MMP-9) slides were photographed in photomicroscope (Carl Zeiss - JVC TK-1270 color video camera) in 400 magnification. Images were quantified using GraphPad Prism Version 8.0

Blue stained area in Masson's trichrome and pink stained area in PAS were considered. Brownish staining was considered as immune-marked to anti-TNF-α, Mmp-9 (Figure 1).

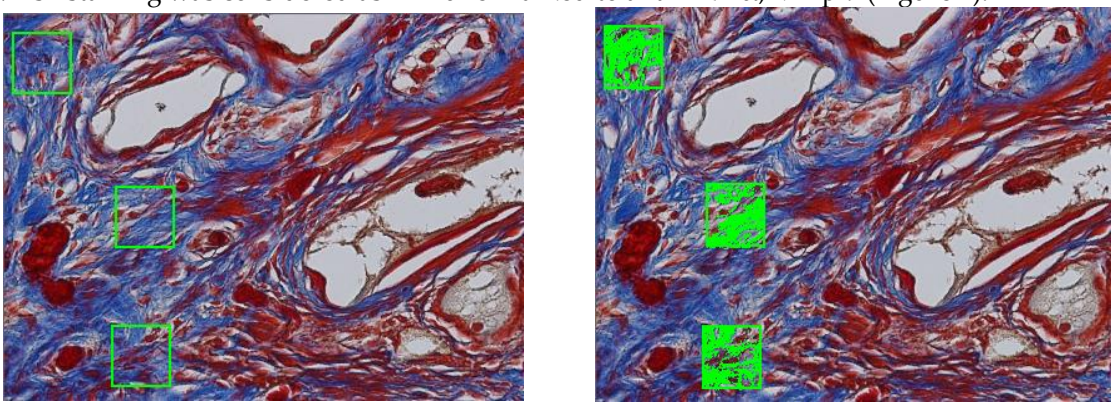

Figure 1. Histomorphometric analysis performed on the Masson's trichrome stained slide.

2.7. Statistical analysis

Data were analyzed using one-way ANOVA, followed by a Wilcoxon Matched-Pairs test ($p < 0.05$). All Analysis were performed by specific softwares (GraphPad Prism Version 8.0 and BioEstat 5.0) (Figure 2).

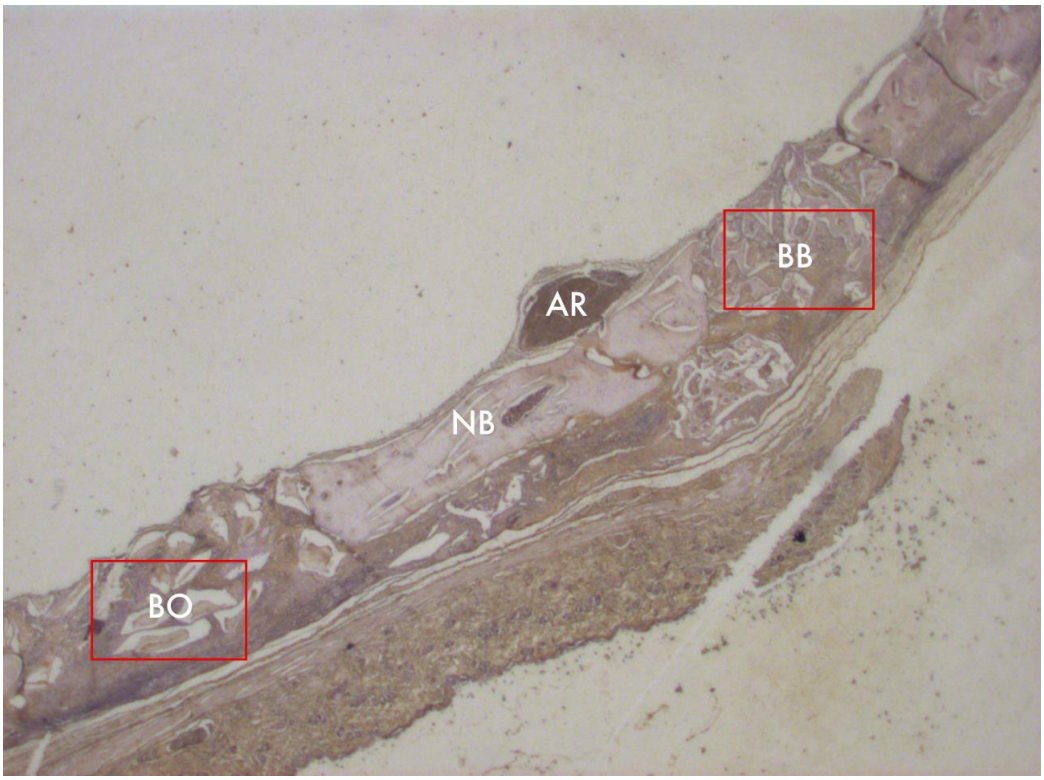

Figure 2. Photomicrograph of animal calvaria sample 8 weeks after surgery. 1-25x magnification. BO = Bio oss; BB = Blue Bone; NB = Native Bone; AR = Artery.

2.8. Scanning electron microscopy protocol

Immediately after euthanization, animal heads were trimmed, surgical sites of biomaterial insertion were re-exposed and immersed in glutaraldehyde (2,5%) in sodium cacodylate buffer (0,1M) at pH 7,4, temperature set at 48º C for 12 hours. Post-fixation included osmium tetroxide (1,0%) and potassium ferrocyanide (0,8%) in cacodylate buffer (0,1M) for 1 hour in dark room. Three changes of sodium cacodylate buffer (0,2M) in distilled water (pH 7,4) for 1h followed. After rinse, specimens were dehydrated in sequential ethanol grades (25-100%). Specimens were immersed in hexamethyldisilazane (10 minutes) and placed inside an evaporation chamber for drying. Colloidal silver adhesive was used to mount specimens on aluminum stubs (Electron Microscopy Sciences, USA). Critical point was achieved (Critical Point Dryer – CPD 030, Bal-Tec, Germany) and specimens were sputter-coated with gold (Cool Sputter Coater – SCD 005, Bal-Tec, Germany).

2.9. Scanning electron microscopy analysis

Coated surfaces were observed and described under a scanning electron microscope (Quanta 250 FEV, Thermo Fischer Scientific, USA) by two experienced, precalibrated, blinded evaluators. Magnifications evaluated were: 5.000X to evaluate biomaterial homogeneity, 15.000X to evaluate cell clusters and architecture, 20.000X to evaluate specific cell types.

3. Results

3.1. General observations

Animals didn't show pain related behavior or feeding/drinking disturbances. Skin wounds healed and hair started to grow over healed wounds.

All 24 animals were sacrificed 60 days after the bone defect procedures. No signs of hemorrhage, no edema or infection were observed.

3.2. Masson's trichrome histomorphometry

Masson's trichrome showed bluish areas in the bone matrix due to aniline blue chemical affinity to collagen fibrils, suggesting new bone formation, as observed in photomicrographs of the central region of newly formed bone. In Group 2 (Blue Bone™) very few or no evidence of the biomaterial was observed. A large area of blue staining was evident and a rich vascular bed, frequently full of blood cells was also observed. On the other hand, in Group 1 (Bio Oss™), very few blue areas are were observed, biomaterial is was easily observed and vascular bed was ferly discrete. (Figure 3).

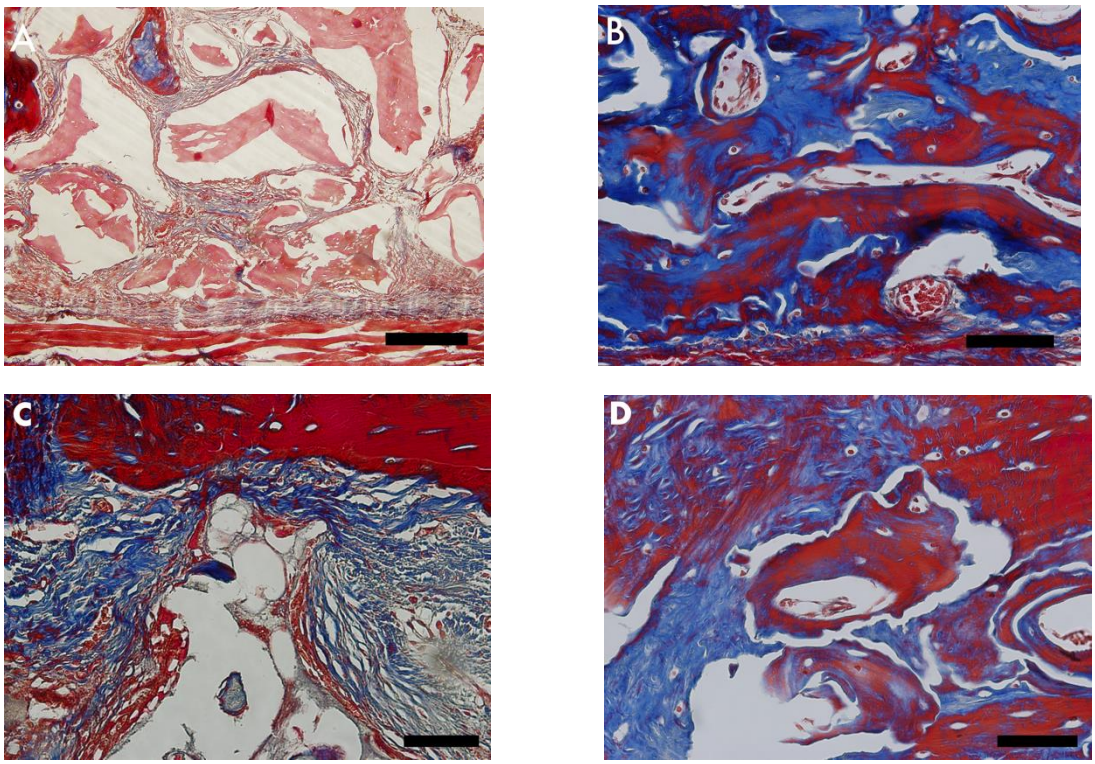

Figure 3. Photomicrographs of Masson's trichrome stained slides. Bluish color indicates collagen fibrils in bone matrix. (A) Group 1 (Bio Oss™), (B) Group 2 (Blue Bone™). Scale bar = 100µm, 400x magnification.

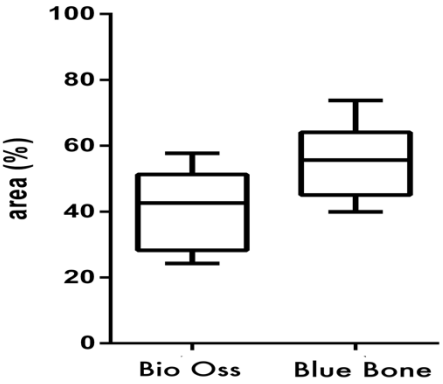

Histomorphometric analysis of Masson's trichrome staining showed higher collagen content in Group 2 (Blue Bone™) than in Group 1 (Bio Oss™). A statistical difference was also found between Group 1 (Bio Oss™) and Group 2 (Blue Bone™) (Graphic 1) and (Table 1).

Table 1. The Masson's trichrome technic analysis, through the Wilcoxon matched-pairs signed rank test showed a statistically significant difference between Group 1 and Group 2.

Wilcoxon matched-pairs signed rank test

P value	0,0313
Exact or approximate P value?	
	Exact
P value summary	
	*
Median of differences	
Median	14,73
How effective was the pairing?	
rs (Spearman)	0,8857
P value (one tailed)	0,0167

3.3. PAS histomorphometry

PAS method was based in, Schiff's periodic acid oxidizing hydroxyl and amino/alkyl amines chemical groups, forming a magenta colored complex. It detected polysaccharides, glycoproteins and glycolipids, suggesting new bone formation. In Group 2 (Blue Bone™) a ferly intense magenta staining was observed. It was concentrated in new-bone matrix borders. In Group 1 (Bio Oss™), in addition to a lightly magenta staining, tissue architecture differs. Higher cell concentration and close proximity of them, suggested an immature bone tissue formation (Figure 4).

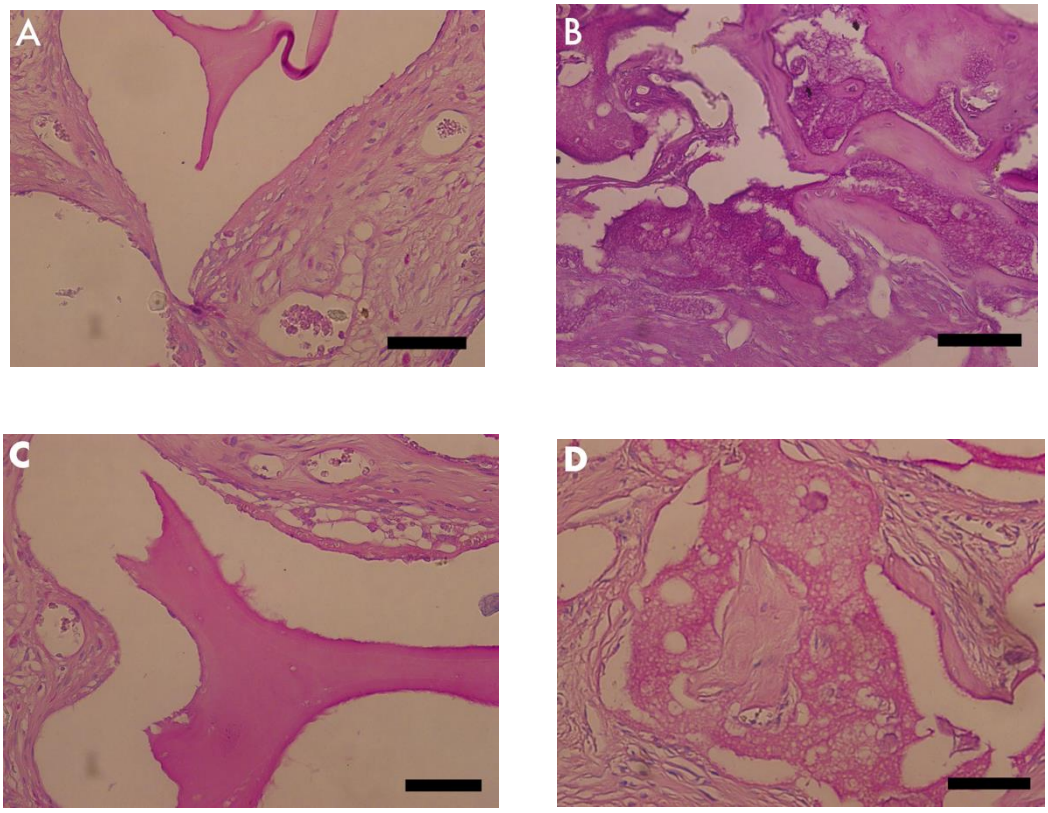

Figure 4. Photomicrographs PAS stained slides. The pink color indicated precursors of the bone matrix. (A) Group 1 (Bio Oss™), (B) Group 2 (Blue Bone™). Scale bar = 100 μm, 400× magnification.

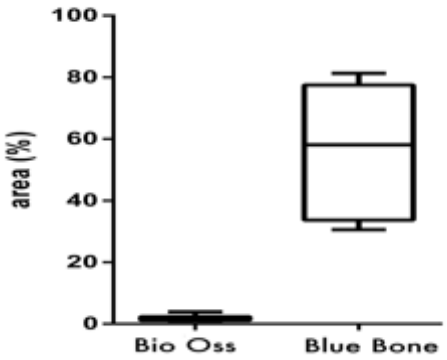

Histomorphometric analysis of PAS staining showed higher polysaccharides, glycoproteins and glycolipid content in Group 2 (Blue Bone™) than Group 1 (Bio Oss™). A statistical difference was also found between Group 1 (Bio Oss) and Group 2 (Blue Bone) (Graphic 2) and (Table 2).

Table 2. It was possible to observe in the PAS analysis, through the Wilcoxon matched-pairs signedrank test, a statistically significant difference between Group1 and Group 2.

Wilcoxon matched-pairs signed rank test	
P value	0,0313
Exact or approximate P value?	
	Exact
P value summary	
	*
Median of differences	
Median	55,23
How effective was the pairing?	
rs (Spearman)	0,5429
P value (one tailed)	0,1486

3.4. TNF-α immunostaining

TNF-α was identified as light brown deposits inside cells and bone matrix. In Group 2 (Blue Bone™) a more intense immunostaining signal was observed in bone matrix, mainly in locations more densely crowded with cells. In Group 1 (Bio Oss™) immunostaining signal was more disperse and less related to cell concentrations. (Figure 5

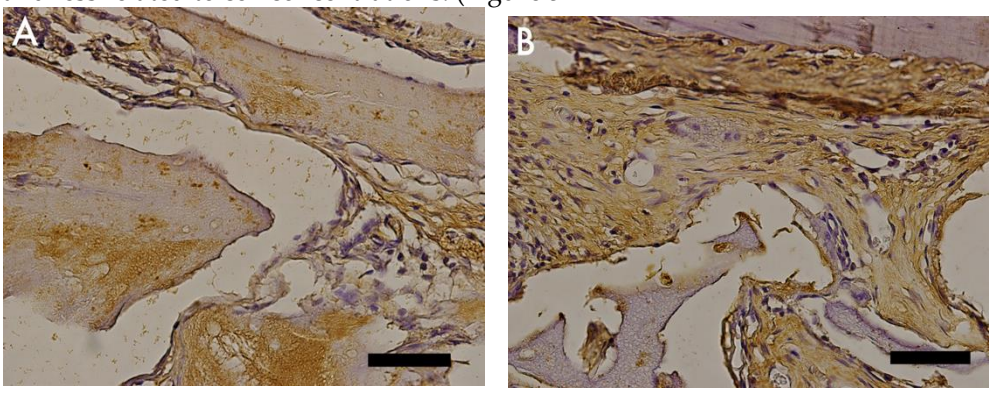

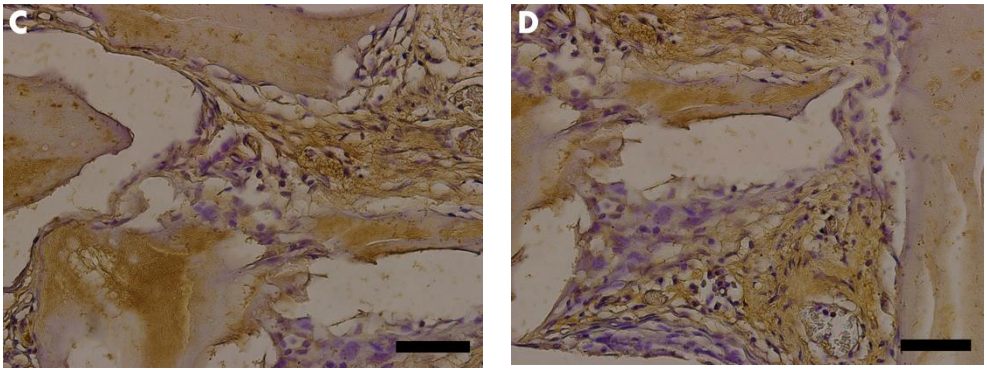

Figure 5. Photomicrographs of TNF-α stained slides. Brown color indicated osteoclast activity. (A) Group 1 (Bio Oss™), (B) Group 2 (Blue Bone™). Scale bar = 100µm, 400x magnification.

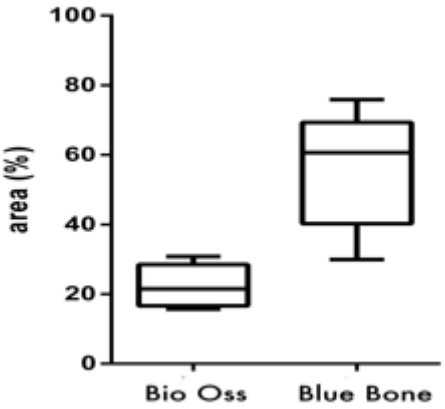

A statistical difference was also found between Group 1 (Bio Oss) and Group 2 (Blue Bone) (Graphic 3), signaling greater cellular activity in Group 2.

Table 3. It was possible to observe in the analysis of TNF-α, through the Wilcoxon matched-pairs signed rank test, a statistically significant difference between Group 1 and group 2.

Wilcoxon matched-pairs signed rank test	
P value	0,0313
Exact or approximate P value?	
	Exact
P value summary	
	*
Median of differences	
Median	38,94
How effective was the pairing?	
rs (Spearman)	-0,6
P value (one tailed)	0,1208

3.5. MMP-9 immunostaining

MMP-9 was identified as light brown deposits inside cells and bone matrix. In Group 2 (Blue Bone™) immunostaining signal was ferly intense and located in extracellular matrix closer to cell crowds. Cell-free matrix was essentially devoid of signal. In Group 1 (Bio Oss™), an evident immunostaing signal also was observed, however, it was concentrated in a few areas (Figure 6).

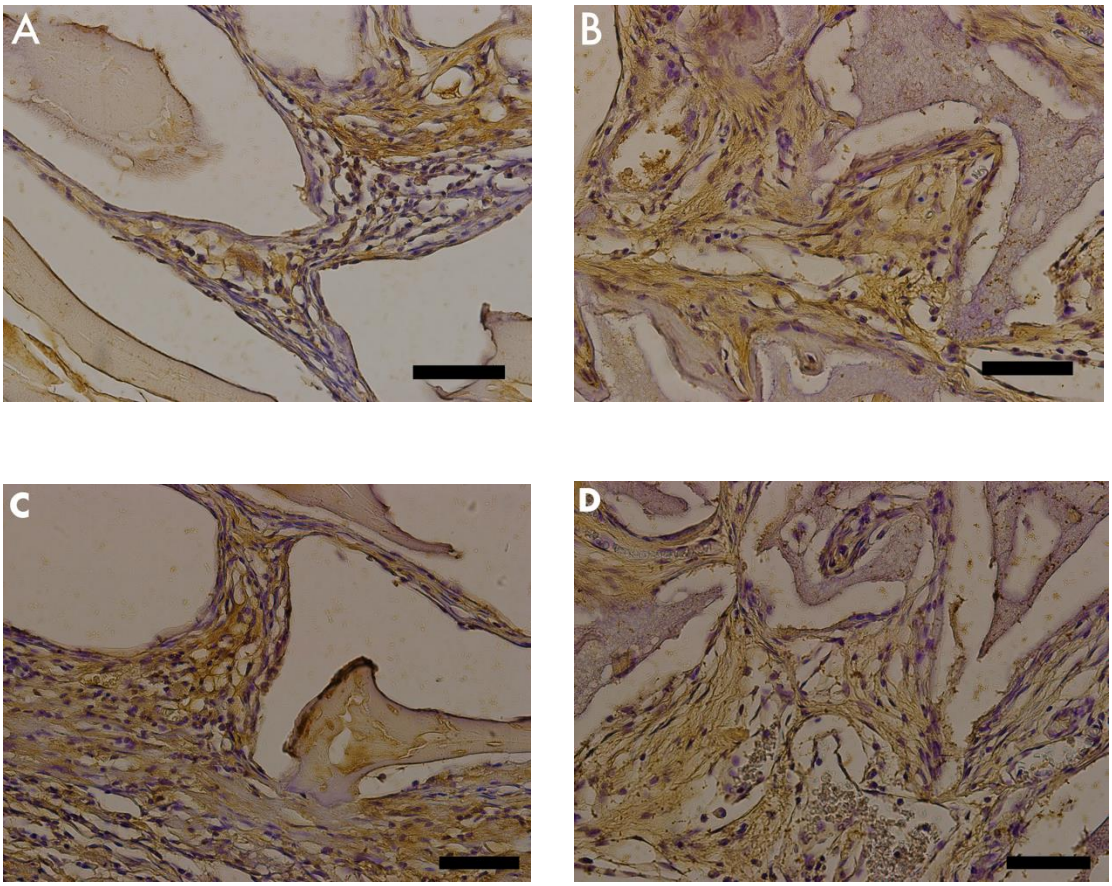

Figure 6. Photomicrographs of MMP-9 stained slides. Brown color indicated osteoblastic activity. (A) Group 1 (Bio Oss™), (B) Group 2 (Blue Bone™). Scale bar = 100μm, 400x magnification. .

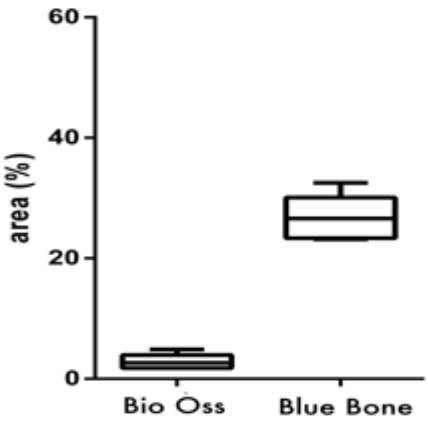

Histomorphometric analysis of MMP=9 staining showed that Group 2 (Blue Bone™) had a higher immunostained area in comparison to Group 1 (Bio Oss™).

Table 4. It was possible to observe in analysis of MMP-9, through the Wilcoxon matched-pairs. Signed rank test, a statistically significant difference between Groups 1 and Group 2.

Wilcoxon matched-pairs signed rank test	
P value	0,0313
Exact or approximate P value?	
	Exact
P value summary	
	*
Median of differences	
Median	24,59
How effective was the pairing?	
rs (Spearman)	-0,3143
P value (one tailed)	0,2819

3.6. Scanning electron microscopy

In scanning electron photomicrographs it was possible to identify the fibroblast after the osseointegration process. Fibroblast displayed the classical flat and spindle shape, with cytoplasm projections following collagen bundles. In addition, fine collagen fibrils could be solely observed or in conjunction with other types of matrix proteins. They formed a reticular structure mainly in matrix borders (Figure 7).

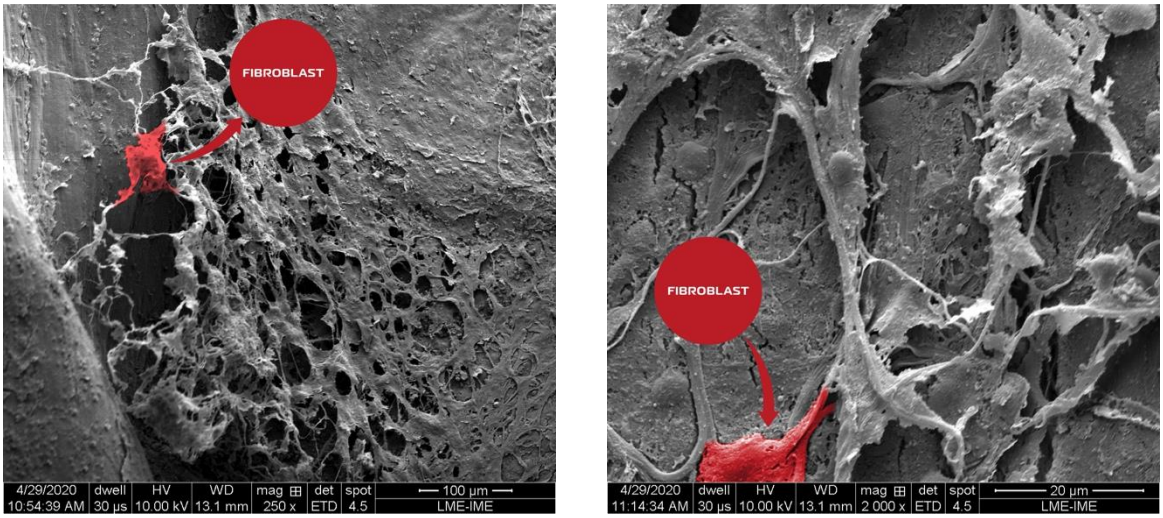

4. Discussion

Worldwide advance in the field of biomaterial research is propelled to the great need for surgical interventions with the use of some biomaterial that harbors specific properties. Several authors have been researching new alternatives that provide more favorable cellular responses. [23,24]

In this respect, our study tested a new nano-HA/β-TCP compound (Blue Bone™) against a longtime successful used biomaterial, xenogenic HA (Bio Oss™), that has gathered an extensive literature to support it during this long period. [3,4,5,6]. We found that some inflammatory mediator and enzyme, related to bone matrix remodeling, were more promptly expressed in nano-HA/β-TCP compound, supporting histological findings that suggested an improvement in new bone matrix production over xenogenic HA, in experimental conditions.

Calvarial bone defects have been used in the last 35 years as *in vivo* model study to evaluate and compare bone replacement materials and regenerative materials [25].

A study of rat calvaria assessed the effectiveness of bone reconstruction by using a variety of biomaterials: bovine bone (refined hydroxyapatite (HA), demineralized bone matrix (DBM) and purified bone collagen (COLL). It was concluded that the HA and DBM powder extracted from bovine bone tissue could also be used for bone defect repair and demonstrated enough potential to be used in clinical studies [26]. Results of the herein study, similarly, indicated that conjunction of different biomaterials (nano-HA with β-TCP) presented a more favorable result than using micrometric hydroxyapatite alone.

Comparative biomaterial study conducted by Anghelescu et al, albeit in rat tibial bone, demonstrated that xenogenic HA (Bio Oss™) and β-TCP exhibited higher platelet endothelial cell adhesion molecule (PECAM 1) and vascular endothelial growth factor (VEGF) immunelabeling than other types of bioactive glasses [27].

Vascularization remains one of the obstacles that need to be overcame in the bone graft design research field [28]. In this respect, the initial nano-HA/β-TCP compound (Blue Bone™) characterization study conducted by da Silva Brum et al., showed a large presence of vascular channels, which indicated that its nanometric structure had a positive result for the creation of blood channels [29].

Masson's trichrome staining was used in the herein study to quantify organic matrix formed between pure bovine HA group and nano-HA/β-TCP compound. It was found statistical difference, signaling that nanotechnology together with the union of the two biomaterials, favors cell proliferation [30]. Another study using similar approach, (HE and Masson's trichrome staining) in rat calvaria, evaluated bone growth in pure hydroxyapatite (HA) and hydroxyapatite (HA) with the addition of wollastonite-hydroxyapatite grafts. Authors found that wollastonite-hydroxyapatite group had more favorable bone growth [31].

Pang et al, in an *in vitro* inflammation essay, revealed that HA particles positively regulate the expression of cytokines IL-1β, TNF-α, IL-6, IL-10, IFN-γ and IL-2 [32]. TNF-α up-regulation was found in this study as well, corroborating Pang et al. findings, albeit using different technic (immunohistochemistry) and extended the up-regulation profile, including MMP-9. These results were also corroborated by another study that evaluated the cellular response of macrophages and osteoclasts, stating that hydroxyapatite could regulate the secretion of TNF-α and IL-6 by macrophages, which would directly affect osteoclast activity in relation to bone resorption [33].

Schiff's periodic acid (PAS) is common tool in investigations related to bone tissue. In a study using pure hydroxyapatite and bioglass in rat calvaria and HE staining to evaluate bone regeneration, in addition to PAS staining to quantify the area of blood vessels, it was found that bioglass provided a better formation of blood vessels than pure hydroxyapatite [34]. These findings are in accord with the herein study which demonstrated a more intense PAS staining in nano-HA/β-TCP compound group than xenogenic HA group. These results suggested further research of bioglass and nano-HA, in order to better understand cell activation between these materials.

Optimizing bone regeneration is a strategic tool, notably in implantology, to circumvent some critical clinical situations, like: atrophic alveolar ridges. Increased alveolar ridges and maxillary sinus lift elevation are common approaches in these situations that are based on the bone inducing biomaterial potential. Grassi et al. restored an atrophic maxillary crest of a 52-year-old woman using a custom-designed lyophilized bone obtained from the corpse donor's tibial hemi-plateau. The authors demonstrated a reduced rate of bone reabsorption after the installation of the graft and implant [35]. A sinus lift was conducted, also in human subject, using nano-HA/β-TCP compound (Blue Bone™) and successfully achieve new bone formation and implants installation [30]. Nanoscaffolds for alveolar bone regeneration is an overly active research field. Different compositions and forms of nanomaterials have been tested, like: nanoparticles, nanofibers,

nanotubes, nanosheets and nanospheres, and they are, frequently associated with growth factors [36].

Sixty days only evaluation period and a limited profile of cell mediator could be considered the main limitations of the study.

5. Conclusion

In conclusion:

- Nano-HA/β-TCP compound presented better condition for bone matrix formation when compared to xenogenic HA.

- MMP-9 and TNF-α up-regulation suggested that cellular response to the bone remodeling process was more favorable in Nano-HA/β-TCP compound group.

- PAS staining technique, suggested Nano-HA/β-TCP compound induced an increase of glycoproteins, polysaccharides and glycolipids.

- Nano-HA/β-TCP compound is a promise biomaterial option to replace xenogenic HA.

References

1. Han Y, Li S, Cao X, Yuan L, Wang Y, Yin Y, Qiu T, Dai H, Wang X. Different inhibitory effect and mechanism of hydroxyapatite nanoparticles on normal cells and cancer cells in vitro and in vivo. Different inhibitory effect and mechanism of hydroxyapatite nanoparticles on normal cells and cancer cells in vitro and in vivo. *Sci Rep*. **2015**, 5, 7943.
2. Yanhua W, Hao H, Li Y, Zhang S. Selenium-substituted hydroxyapatite nanoparticles and their in vivo antitumor effect on hepatocellular carcinoma. *Colloids Surf B Biointerfaces*. **2016**, 140, 297-306.
3. Aludden HC, Mordenfeld A, Hallman M, Dahlin C, Jensen T. Lateral ridge augmentation with Bio-Oss alone or Bio-Oss mixed with particulate autogenous bone graft: a systematic review. *Int J Oral Maxillofac Surg*. **2017**, 46(8), 1030-1038.
4. Akbarzadeh Baghban A, Dehghani A, Ghanavati F, Zayeri F, Ghanavati F. Comparing alveolar bone regeneration using Bio-Oss and autogenous bone grafts in humans: a systematic review and meta-analysis. *Iran Endod J*. **2009,** 4(4), 125-30.
5. Jensen T, Schou S, Stavropoulos A, Terheyden H, Holmstrup P. Maxillary sinus floor augmentation with Bio-Oss or Bio-Oss mixed with autogenous bone as graft: a systematic review. *Clin Oral Implants Res*. **2012**, 23(3), 263-73.
6. Jensen T, Schou S, Stavropoulos A, Terheyden H, Holmstrup P. Maxillary sinus floor augmentation with Bio-Oss or Bio-Oss mixed with autogenous bone as graft in animals: a systematic review. *Int J Oral Maxillofac Surg*. **2012**, 41(1), 114-20.
7. Song JE, Tripathy N, Lee DH, Park JH, Khang G. Quercetin Inlaid Silk Fibroin/Hydroxyapatite Scaffold Promotes Enhanced Osteogenesis. *ACS Appl Mater Interfaces*. **2018**, 10(39), 32955-32964.
8. Sadowska JM, Wei F, Guo J, Guillen-Marti J, Lin Z, Ginebra MP, Xiau Y. The effect of biomimetic calcium deficient hydroxyapatite and sintered β-tricalcium phosphate on osteoimmune reaction and osteogenesis. *Acta Biomater*. **2019**, 96, 605-618.
9. Ngiam M, Nguyen LT, Liao S, Chan CK, Ramakrishna S. Biomimetic nanostructured materials: potential regulators for osteogenesis?. *Ann Acad Med Singapore*. **2011**, 40(5), 213-222.
10. Sadowska JM, Wei F, Guo J, Guillem-Marti J, Ginebra MP, Xiao Y. Effect of nano-structural properties of biomimetic hydroxyapatite on osteoimmunomodulation. *Biomaterials*. **2018**, 181, 318-332.
11. Bradfield J. Identifying animal taxa used to manufacture bone tools during the Middle Stone Age at Sibudu, South Africa: Results of a CTrendered histological analysis. *PLoS ONE* **2018**, 13(11), e0208319.
12. Ismail FW, Shamsudin AM, Wan Z, Daud SM, Samarendra MS. Ki-67 immuno-histochemistry index in stage III giant cell tumor of the bone. *J Exp Clin Cancer Res*. **2010**, 29:25,

13. Singh T, Chandu A, Clement J, Angel C. Immunohistochemistry of Five Molecular Markers for Typing and Management of Ameloblastomas: A Retrospective Analysis of 40 Cases. *J Maxillofac Oral Surg*. **2017**, 16(1), 65-70.
14. Zyada MM. Expression of matrix metalloproteinase-9 and significance of a macrophage assay in eosinophilic granuloma. *Ann Diagn Pathol*. **2009**, 13(6), 367-372.
15. Nielsen BS, Sehested M, Kjeldsen L, Borregaard N, Rygaard J, Danø K. Expression of matrix metalloprotease-9 in vascular pericytes in human breast cancer. *Lab Invest*. **1997**, 77(4), 345-355.
16. Zambuzzi WF, Paiva KB, Menezes R, Oliveira RC, Taga R, Granjeiro JM. MMP-9 and CD68(+) cells are required for tissue remodeling in response to natural hydroxyapatite. *J Mol Histol*. **2009**, 40(4), 301-309.
17. Jo YY, Kim SG, Kwon KJ, Kweon HY, Chae WS, Yang WG, Lee EY, Seok H. Silk Fibroin-Alginate-Hydroxyapatite Composite Particles in Bone Tissue Engineering Applications In Vivo. *Int J Mol Sci*. **2017**, 18(4), 858.
18. Liu H, Xu GW, Wang YF, Zhao HS, Shiong S, Wu Y, Heng BC, An CR, Zhu GH, Xie DH. Composite scaffolds of nano-hydroxyapatite and silk fibroin enhance mesenchymal stem cell-based bone regeneration via the interleukin 1 alpha autocrine/paracrine signaling loop. *Biomaterials*. **2015** 49, 103-112.
19. Pal R, Mamidi MK, Das AK and Bhonde R: Diverse effects of dimethyl sulfoxide (DMSO) on the differentiation potential of human embryonic stem cells. *Arch Toxicol.* **2012**, 86, 651-661.
20. Hui H, Ma W, Cui J, Gong M, Wang Y, Zang Y, Ne T, Bi Y, He Y. Periodic acid-Schiff staining method for function detection of liver cells is affected by 2% horse serum in induction médium. *Mol Med Rep*. **2017**, 16, 8062-8068.
21. S. G. Velleman. The Role of the Extracellular Matrix in Skeletal Development. *Poult Sci*. **2000,** 79, 985–989.
22 Prokop M, Gut D, Nowak MP. Scanning gate microscopy mapping of edge current and branched electron flow in a transition metal dichalcogenide nanoribbon and quantum point contact. *J Phys Condens Matter*. **2020**, 13, 205302.
23. Sobczak-Kupiec, A.; Kowalski, Z.; Wzorek, Z. Preparation of hydroxyapatite from animal bones. *Acta Bioeng Biomech*. **2009**, 11, 23–28.
24. K.; Murata, K.; Omokawa, S.; Akahane, M.; Shimizu, T.; Kawamura, K.; Kawate, K.; Tanaka, Y. Promotion of Osteogenesis and Angiogenesis in Vascularized Tissue-Engineered Bone Using Osteogenic Matrix Cell Sheets. *Plast Reconstr Surg*. **2016**, 137, 1476–1484.
25. Cooper GM, Mooney MP, Gosain KA, Campbell PG, Losee JE, Huard J. Testing the critical size in calvarial bone defects: revisiting the concept of a critical-size defect. *Plast Reconstr Surg*. **2010**, 125(6), 1685-1692.
26. Veremeev, A.; Bolgarin, R.; Nesterenko, V.; Andreev-Andrievskiy, A.; Kutikhin, A. Native Bovine Hydroxyapatite Powder, Demineralised Bone Matrix Powder, and Purified Bone Collagen Membranes are Efficient in Repair of Critical-Sized Rat Calvarial Defects. *Materials.* **2020**, 13, 3393.
27. Anghelescu VM, Neculae I, Dincă O, Vlădan C, Socoliuc C, Cioplea M, Nichita L, Popp C, Zurac S, Bucur A.Inflammatory-Driven Angiogenesis in Bone Augmentation with Bovine Hydroxyapatite, B-Tricalcium Phosphate, and Bioglasses: A Comparative Study. *J Immunol Res*. **2018**, 12, 9349207.
28. Mirjam Fröhlich et all 2008. Tissue Engineered Bone Grafts: Biological Requirements, Tissue Culture and Clinical Relevance. *Curr Stem Cell Res Ther*. **2008**, 3(4), 254–264.
29. da Silva Brum I, de Carvalho JJ, Pires JLS, de Carvalho MAL, Santos LBF, Elias CN. Nanosized hydroxyapatite and β-tricalcium phosphate composite: physico-chemical, cytotoxicity, morphological properties and *in vivo* trial. *Sci Rep*. **2019**, 9, 19602.
30. Amorim Lopes JC, Salviano SH, Lins CAB, Devita RL, Carvalho JJ, da Silva Brum I, Fernandes GVO. Histological and Immunohistochemical Analysis of a Nanobiomaterial in a Maxillary Sinus Lift Surgery: A Case Report. *Br J Med Health Res*. **2020**, 7(07), 13-27.
31. Ge R, Xun C, Yang J, Jia W, Li Y. In vivo therapeutic effect of wollastonite and hydroxyapatite on bone defect. *Biomed Mater*. **2019**, 14(6), 065013.
32. Pang S, Li X, Wu D, Li H, Wang X. Tuning inflammation response via adjusting microstructure of hydroxyapatite and biomolecules modification. *Colloids Surf B Biointerfaces*. **2019**, 177, 496-505.
33. Pasuri J, Holopainen J, Kokkonen H, Persson M, Kauppinen K, Lehenkari P, Santala E, Ritala M, Tuukkanen J. Osteoclasts in the interface with electrospun hydroxyapatite. *Colloids Surf B Biointerfaces*. **2015,** 135, 774-783.

34. Bi L, Jung S, Day D, Neidig K, Dusevich V, Eike D, Bonewald L. Evaluation of bone regeneration, angiogenesis, and hydroxyapatite conversion in critical-sized rat calvarial defects implanted with bioactive glass scaffolds. *J Biomed Mater Res A*. **2012**, 100(12), 3267-3275.

35 Grassi FR, Grassi R, Vivarelli L, Dallari D, Govoni M, Nardi GM, Kalemaj Z, Ballini A. Design Techniques to Optimize the Scaffold Performance: Freeze-dried Bone Custom-made Allografts for Maxillary Alveolar Horizontal Ridge Augmentation. *Materials*. **2020**, 13(6), 1393.

36 Funda G, Taschieri S, Bruno GA, Grecchi E, Paolo S, Girolamo D, Del Fabbro M. Nanotechnology Scaffolds for Alveolar Bone Regeneration. *Materials*. **2020**, 13(1), 201.